AD_____

Award Number: DAMD17-00-1-0291

TITLE: A Training Program in Breast Cancer Research Using NMR Techniques

PRINCIPAL INVESTIGATOR: Paul C. Wang, Ph.D.

CONTRACTING ORGANIZATION:

Howard University
Washington, DC 20059

REPORT DATE: July 2002

TYPE OF REPORT: Annual

PREPARED FOR: U.S. Army Medical Research and Materiel Command
Fort Detrick, Maryland 21702-5012

DISTRIBUTION STATEMENT: Approved for Public Release;
Distribution Unlimited

The views, opinions and/or findings contained in this report are those of the author(s) and should not be construed as an official Department of the Army position, policy or decision unless so designated by other documentation.

REPORT DOCUMENTATION PAGE

Form Approved
OMB No. 074-0188

1. AGENCY USE ONLY (Leave blank)	2. REPORT DATE	3. REPORT TYPE AND DATES COVERED
	July 2002	Annual (1 Jul 01 - 30 Jun 02)

4. TITLE AND SUBTITLE
A Training Program in Breast Cancer Research Using NMR Techniques

5. FUNDING NUMBERS
DAMD17-00-1-0291

6. AUTHOR(S)
Paul C. Wang, Ph.D.

7. PERFORMING ORGANIZATION NAME(S) AND ADDRESS(ES)
Howard University
Washington, DC 20059

E-Mail: pwang@howard.edu

8. PERFORMING ORGANIZATION REPORT NUMBER

9. SPONSORING / MONITORING AGENCY NAME(S) AND ADDRESS(ES)
U.S. Army Medical Research and Materiel Command
Fort Detrick, Maryland 21702-5012

10. SPONSORING / MONITORING AGENCY REPORT NUMBER

11. SUPPLEMENTARY NOTES
Report contains color

12a. DISTRIBUTION / AVAILABILITY STATEMENT
Approved for Public Release; Distribution Unlimited

12b. DISTRIBUTION CODE

13. ABSTRACT *(Maximum 200 Words)*

In the second year, this program has supported two graduate students (one from the Electrical Engineering Department and one from the Biochemistry Department) and three postdoctoral fellows (Radiology Department). This program supports the graduate students in the second year. The new postdoctoral fellows have been introduced to the Biomedical NMR Laboratory and the Howard University Cancer Center. The trainees have continued to learn the theory and instrumentation of nuclear magnetic resonance imaging and spectroscopy. The trainees have rotated through the mammography service in the Department of Radiology in the hospital to learn the mammography procedures. Besides attending the weekly seminars in the Cancer Center, the trainees also have attended a special seminar series on the breast imaging sponsored by this grant and the Department of Electrical Engineering. The trainees have actively participated in several research projects. Based on the experimental findings, one paper was published and three posters have been presented in the national scientific meetings. Two graduate student trainees have passed their comprehensive exams and have started research for their Ph.D. thesis. One postdoctoral trainee has completed his radiology resident training. The PI has submitted a NIH grant as a co-investigator.

14. SUBJECT TERMS	15. NUMBER OF PAGES
breast cancer, training, nuclear magnetic resonance	17
	16. PRICE CODE

17. SECURITY CLASSIFICATION OF REPORT	18. SECURITY CLASSIFICATION OF THIS PAGE	19. SECURITY CLASSIFICATION OF ABSTRACT	20. LIMITATION OF ABSTRACT
Unclassified	Unclassified	Unclassified	Unlimited

TABLE OF CONTENTS

IV. Reports

There are two Ph.D. graduate students (Emmanuel Agwu and Lisa Kinnard) and three postdoctoral research associates (Yusuf Ali, Huafu Song and Renshu Zhang) supported by this grant. Emmanuel Agwu is a 6th yr MD/PhD student pursuing his Ph.D. degree in Biochemistry. Lisa Kinnard is a graduate student from the Department of Electrical Engineering. Yusuf Ali is a resident in the Department of Radiology. Renshu Zhang is a radiologist by training. Huafu Song is a NMR/MRI specialist.

The trainees have rotated through the mammography service in the Department of Radiology in the hospital to learn the mammography procedures. Besides attending the weekly seminars in the Cancer Center, the trainees also have attended a special seminar series on the breast imaging sponsored by this grant and the Department of Electrical Engineering. The trainees have actively participated in several research projects. Based on the experimental findings, one paper was published and three posters have been presented in the national scientific meetings. Two graduate student trainees have passed their comprehensive exams and have started research for their Ph.D. thesis. One postdoctoral trainee has completed his radiology resident training. The PI has submitted a NIH grant as a co-investigator.

Statement-of-Work Year 2:

- **Take departmental comprehensive exams**
  Both Emmanuel Agwu and Lisa Kinnard have passed their comprehensive exams.
- **Submit a five page pre-proposal 30 days before taking comprehensive exam**
  Both Emmanuel Agwu and Lisa Kinnard have submitted pre-proposals as required by the Electrical Engineering Department and the Biochemistry Department.
- **Write an expanded research proposal and defend the proposal**
  The proposals submitted by both students have been accepted.
- **Once the student has passed the written and oral comprehensive exams, the student is qualified as a Ph.D. candidate**
  Both students are Ph.D. candidates.
- **Select a thesis committee**
  Emmanuel Agwu's thesis committee members are: Drs. C. Coomes, J. Mack, A. Rhoads, and P. Wang. The committee has met twice reviewing Emmanuel Agwu progress.
  Lisa Kinnard's thesis committee members are: Drs. M. Chouikha, B. Lo, T. Gill, A. Rubaai, and P. Wang. The committee has met three times reviewing Lisa Kinnard's progress.
- **Start thesis project**
  Both students have started their Ph.D. thesis projects.
- **Report to MD/Ph.D. committee and respective department on research progress each semester**
  Both students have submitted written progress reports.
- **Clinical preceptorship one half day per week**
  Lisa Kinnard has worked with Dr. Eva Duckett of the Howard University Hospital Radiology department. During this internship, Dr. Duckett trained her in the

following areas: 1) Patient management, 2) Screening/Diagnostic procedure, 3) Breast cancer image patterns, 4) Understanding of typical cases versus clinically indeterminate cases, 5) Understanding of geometric distribution (physical locations of tumors), 6) Image patterns of cysts, fibroadenomas, 7) Image pattern analysis of masses vs. microcalcifications and 8) Biopsy procedures.
Emmanuel Agwu is in his 4th medical school training, which is a clinical rotation for the whole year.

Postdoctoral Student:

Year 2:

- **Participate in weekly Cancer Center Seminars**
  All the postdocs and graduate students participated weekly Cancer Center seminars. With the Electrical Engineering Department, the Biomedical NMR Laboratory started series seminars on breast imaging. This seminar series is partially support by this grant. A list of seminars is attached in the appendix.
- **Organize weekly research group meeting**
  The lab has a regular weekly group meeting discussing the progress of experiments.
- **Continue research project**
  The research associates have presented a poster in at the AACR Molecular Imaging meeting.
- **Present progress report to the Executive Committee**
  The Executive Committee has reviewed and satisfied the progress of research.
- **Clinical preceptorship one half day per week**
  Ali Yusuf is a radiology resident. He has clinical responsibility everyday. RenShu Zhang is a radiologist by training and she is familiar with mammography procedures.

V. Reportable Outcomes

Papers:

1. Kinnard L, Lo S-C.B, Wang P, Freedman MT, Chouikha M, Separation of Malignant and Benign Masses in Mammography using Maximum-Likelihood Modeling and Neural Networks. Proc. of SPEI Vol 4684: 733-741, 2002.

Abstracts:

1. Agwu EC, Zhou JW, Sridhar R, Wang PC. An Improved NMR Perfusion System For Breast Cancer Cell Study. Association For Academic Minority Physicians 15th Annual Scientific Meeting, October 12-14, Washington, DC. 2001.
2. Zhang RS, Li EC, Ali YD, Song HF, Fan KJ, Pirollo KF, Chang EH, Wang PC. Dynamic Magnetic Resonance Imaging of Prostate Cancer in Mice. American Association for Cancer Research Conference, Molecular Imaging in Cancer: Linking Biology, Function, and Clinical Application In Vivo, January 23-27, 2002, Orlando, Fl.

3. Kinnard L, Lo S-C.B, Wang P, Freedman MT, Chouikha M, Separation of Malignant and Benign Masses in Mammography using Maximum-Likelihood Modeling and Neural Networks. SPEI Med Imaging, Feb. 2002, San Diego, CA.

Ph.D. Thesis Proposals:

1. Emmanuel Agwu "In Vitro and in Vivo Characterization of MCF7 Sensitive and MCF7 Multidrug Resistant Cell Metabolism Using Magnetic Resonance Spectroscopy" Department of Biochemistry and Molecular Biology
2. Lisa Kinnard "Segmentation Classification of Malignant and Benign Masses in Digital Mammography using Maximum-Likelihood Modeling and Neural Networks." Department of Electrical Engineering

Awards:

1. The PI was chosen as a recipient of an AACR-HBCU Faculty Scholar Award in Cancer Research for the AACR Special Conference entitled "Molecular Imaging in Cancer: Linking Biology, Function, and Clinical Application In Vivo" held January 23-27, 2002 Lake Buena Vista, Fl.

V. Appendix

1. The poster from the AACR Molecular Imaging Conference, "Molecular Imaging in Cancer: Linking Biology, Function, and Clinical Application In Vivo", January 23-27, 2002, Orlando, Fl.
2. The paper published in SPEI Vol 4684: 733-741, 2002.
3. A list of the "Breast Imaging" seminars.

AACR Molecular Imaging Conference, Orlando, Fl, 2002

Dynamic MR Imaging of Prostate Cancer in Mice

Renshu Zhang[1], Ercheng Li[1], Yusuf D. Ali[1], Huafu Song[1], Kuang J. Fan[2], Kathleen F. Pirollo[3], Esther H. Chang[3], Paul C. Wang[1]*

[1]Department of Radiology and Cancer Center, Howard University, Washington, DC.
[2]Department of Pathology, Howard University, Washington, DC.
[3]Department of Oncology, Georgetown University Medical Center, Washington, DC

Introduction

Prostate cancer is the most common malignant tumor and is the second most common cause of cancer related mortality among men. Prostate cancer patients often require frequent imaging follow-up of their tumors. The non-invasive, strong soft-tissue contrast nature, and lack of radiation involvement with MRI make it an ideal choice of imaging method for detection, evaluation, and for routine tumor monitoring. Angiogenesis and neovascularization play an important role in tumor growth and metastasis. Intravascular MR contrast agents could be used to detect the high blood flow, vascular density, and capillary permeability of prostate tumors [1]. More over, dynamic contrast-enhanced MRI demonstrated that the rate of change in signal enhancement is an important parameter for the tumor distinction [2].

Objectives

In this study we performed a dynamic contrast-enhanced MRI study of prostate tumors in athymic nude mice to clarify the mechanism of heterogeneity contrast enhancement of the tumor, to assess the kinetics of contrast enhancement, and to correlate the MR contrast enhancement with histopathological findings.

Materials and Methods

Animal preparation 10^7 prostate cancer cells (DU145) suspended in Matrigel were injected subcutaneously into the lower back near the tail of the nude mice. The athymic nude mouse was chosen in this study, because of its immunodeficiency, and lack of rejection of the inoculated human tumor cells which will be allowed to proliferate. The MRI scan was performed when the tumors grew to approximately 1 cm in diameter. A catheter (potyethylene tubing, 0.6 mm o.d.) was placed in the jugular vein enabling administration of the contrast agent without changing the position of animal within the magnet [Fig.1]. All mice were anesthetized before and during MR scanning with 1.5 ~2 .0 vol % isoflurane mixed with oxygen in a flow rate of 200 cm^3/min through a naso- buccal cone mask. The mouse was put in the lateral decubitus position, inside the magnet (a Varian 4.7 T horizontal bore NMR machine) under the respiration monitoring.

Fig. 1 Post jugular venous catheter insertion.

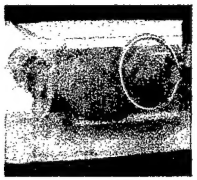

Fig. 2 Mouse in the decubitus position on the cradle and the tumor is positioned at the center of the coil.

MR Imaging procedure A 2.0 cm single loop RF coil was placed around tumor for imaging [Fig. 2]. T1-weighted spin-echo imaging technique with the echo time (TE) 12 ms and the repetition time (TR) 750 ms was used. The image slice thickness was 1 mm, field-of-view (FOV) 2.0 cm, and matrix size 256x200. A set of coronal and transverse images (five slices in each orientation) was taken as baseline before injection of the contrast agent [Fig. 3], Magnevist (Berlex Laboratories Inc.) at 0.4 mmol/kg. During the injection of the contrast agent, a series of fast spin-echo images were acquired. After the completion of injection, a series of T1-weight spin-echo images were obtained every 30 minutes to monitor the dynamic changes of contrast enhancement [Figs. 4, 5 and 6].

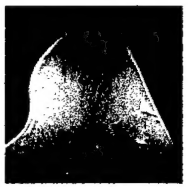

Fig. 3 T1 weighted axial MR image obtained before IV contrast agent injection, demonstrates heterogeneous increased signal intensity of the tumor in comparison to the muscle. The tumor borders are not well defined.

Fig. 4 T1 weighted axial MR image obtained 10 minutes after IV contrast agent injection shows well defined tumor borders and heterogeneous peripheral enhancement of the tumor. There is no enhancement noted in the tumor center.

Fig. 5 T1 weighted axial images obtained 1 hour after IV contrast agent administration depicts more central enhancement of the tumor and decreased enhancement of the tumor periphery.

Fig. 6 T1 weighted MR image obtained 3 hours after IV contrast agent administration shows marked enhancement of the tumor center and notable decreased peripheral enhancement.

Histology specimen preparation The mouse was sacrificed after the completion of the MR imaging. Tumor was dissected and cut in the same plane as the MR images. Photographic images of the gross specimens were obtained [Fig.7]. The tumors were fixed in 4% formaldehyde solution. Several sections of approximately 4-µm thickness were dissected, stained with hemotoxylin-eosinn and embedded in paraffin.

Fig. 7 Gross picture of the tumor showing the heterogeneous appearance of the tumor which has been cut in the same plane as the image.

Fig. 8 Histological details of a highly anaplastic tumor showing large area of necrosis (black arrow). There is markedly increased vascularity in the tumor tissue at the margin of the necrosis (white arrows). (10x4, H&E). The specimen was obtained from area shown by the red square on the MR image (Fig.6).

Fig. 9 Higher magnification of same area depicting abundant capillary channels at the margin of the necrosis (white arrows). (10x10, H&E)

Results and Discussion

The early images during the injection and first 10 minutes show a rapid contrast enhancement in the periphery of the tumors [Fig.4]. The later images showed progressive uneven enhancement throughout the center of the tumor[Figs. 5 and 6]. In the histological specimens [Figs. 8 and 9], the early enhancing peripheral areas corresponded well to regions with dense and highly permeable capillaries. The slow enhancing central regions consisted of areas of cystic and necrotic degeneration of the tumor tissue [Figs. 8]. The slow enhancement of the central areas can be explained by the predominant diffusion of the contrast agent from the highly permeable peripheral regions with high leakage into the cystic and necrotic areas devoid of capillaries [2]. In the literature, the rate and the overall steady state of contrast enhancement have been used to determine the malignancy of tumors[3]. The dynamic contrast-enhanced MR images can be used as a powerful means to characterize tumor prognosis, and to monitor therapeutic responses to chemo, hormonal and radiotherapy [4, 5].

References

1. Fan X., River J. N., et al, (2001) Magn Reson Med. 45, 1046-1055.
2. Furman-Haran, E., Margalit, R. et al. (1996) *Proc. Natl. Acad. Sci. USA.* 93, 6247-6251.
3. Konda SD, Aref M, et al. (2000) Invest Radiol. 35, 50-57
4. Brasch R, Turetschek K. (2000) Eur J Radiol. 34, 148-155.
5. Padhani A.R., Husband J.E.(2001) Clinic Radiology. 56, 607-620

Separation of Malignant and Benign Masses using Maximum-Likelihood Modeling and Neural Networks

Lisa Kinnard[a,b], Shih-Chung B. Lo[a], Paul Wang[c], Matthew Freedman[a], Mohamed Chouikha[b]

[a]ISIS Center, Department of Radiology, Georgetown University Medical Center, Washington, D.C.

[b]Department of Electrical Engineering, Howard University, Washington, D.C., USA

[c]Biomedical NMR Laboratory, Department of Radiology, Howard University, Washington, D.C.

ABSTRACT

This study attempted to accurately segment the masses and distinguish malignant from benign tumors. The masses were segmented using a technique that combines pixel aggregation with likelihood analysis. We found that the segmentation method can delineate the tumor body as well as tumor peripheral regions covering typical mass boundaries and some spiculation patterns. We have developed a multiple circular path convolution neural network (MCPCNN) to analyze a set of mass intensity, shape, andtexture features for determination of the tumors as malignant or benign. The features were also fed into a conventional neural network for comparison. We also used values obtained from the maximum likelihood values as inputs into a conventional backpropagation neural network. We have tested these methods on 51 mammograms using a grouped Jackknife experiment incorporated with the ROC method. Tumor sizes ranged from 6mm to 3cm. The conventional neural network whose inputs were image features achieved an A_z value of 0.66. However the MCPCNN achieved an A_z value of 0.71. The conventional neural network whose inputs were maximum likelihood values achieved an A_z value of 0.84. In addition, the maximum likelihood segmentation method can identify the mass body and boundary regions, which is essential to the analysis of mammographic masses.

Keywords: Computer-assisted diagnosis, breast cancer, convolution neural networks, feature extraction

1. INTRODUCTION

While many breast cancer diagnostic systems have been developed, fully-automated mass segmentation continues to be a major challenge in this area. Several investigators exploited methods using intensity values to decide if a pixel should be placed in the region of interest (ROI) or background [14,9,5,7]. Petrick[12] et al. developed the density weighted contrast enhancement (DWCE) method which applies a series of filters to the image in an attempt to extract masses. Li[6] et al. developed a competetitive classification strategy, which uses a combined soft and hard classification method for deciding if segmented regions are true or false positives. Li[7] et al. developed a segmentation method that uses probability to determine segmentation contours. Most of these methods are successful at segmenting the tumor body, however, they sometimes do not properly obtain the extended boundaries of the tumor. While conventional region-growing is an excellent pixel-based segmentation method, it may not suitable to use this method alone. It produces many segmentation contours for one tumor image, but does not decide which segmentation contour is the best. Based on the above reasons, we have developed a tumor segmentation method that combines region-growing with probability assessment to determine final segmentation contours for various breast tumor images.

The most recognized obstacles in breast cancer diagnosis are (1) difficulties of diagnostic decision making in calling back patient for further breast examination, (2) the large number of suspected lesions of which only part

Further author information: (Send correspondence to Lisa M. Kinnard)
Lisa M. Kinnard: E-mail: kinnard@isis.imac.georgetown.edu, Telephone: 1 202 687 5135
S.C. Ben Lo: E-mail: lo@isis.imac.georgetown.edu, Telephone: 1 202 687 1659,
Address: ISIS, Georgetown University, 2115 Wisconsin Avenue, NW, Washington DC, USA

Medical Imaging 2002: Image Processing, Milan Sonka, J. Michael Fitzpatrick, Editors, Proceedings of SPIE Vol. 4684 (2002) © 2002 SPIE · 1605-7422/02/$15.00

of them are malignant lesions; and (3) missed diagnosis of breast cancer. The callback rates vary from 5% to 20% in today's breast cancer screening programs[1,16]. At some medical centers, the positive predictive rate can be 30% to 35%[4,1]while at others this rate can be as low as 10% to 15%. It is well known that effective treatment of breast cancer calls for early detection of cancerous lesions (e.g., clustered microcalcifications and masses associated with malignant cellular processes)[16,11,15] Tumors can be missed because they are obscured by glandular tissue and it is therefore difficult to observe their boundaries. We were motivated by this clinical obstacle and have developed a computer-assisted diagnostic system attempted to tackle this issue as demonstrated in the following sections.

2. METHODS

Computer-assisted breast cancer diagnosis is divided into three parts, namely, image segmentation, feature calculation, and classification. The next several section will theoretically describe the methods used in the study.

2.1. Segmentation

It is well known that lesion segmentation is one of the most important aspects of computer-assisted diagnosis (CAD_x) because one of the main characteristics of malignant tumors is ill-defined, and/or spiculated borders. Conversely, benign tumors typically have well-defined, rounded borders. Segmentation is therefore extremely important because the diagnosis of a tumor can strongly depend upon image features.

Pixel aggregation is an automated segmentation method in which the region of interest begins as a single pixel and grows based on surrounding pixels with similar properties, e.g., grayscale level or texture.[2] It is a commonly used method[13,14,9]due to its simplicity and accuracy. The computer will use the maximum intensity as the "seed point" -a pixel that is similar to the suspected lesion and is located somewhere inside the suspected lesion. The next 4- or 8-neighboring pixel is checked for similarity so that the region can grow. If pixels in the 4- or 8-neighboring region are similar, they are added to the region. The region continues to grow until there are no remaining similar pixels that are 4- or 8-neighbors of those in the grown region.

Our implementation of this method checks the 4-neighbors of the seed pixel and uses a graylevel threshold as the similarity criterion. If a 4-neighbor of a pixel has an intensity value greater than or equal to a set threshold, it is included in the region of interest. The 4-neighbors were checked instead of the 8-neighbors so that surrounding tissue will not be included. The intensity threshold was used as a similarity criterion due to its simplicity and effectiveness.

By using the same seed point with multiple intensity threshold values we obtained between 150 and 300 of gray level change per lesion; however, the computer did not have the ability to choose the best partition. We added a maximum-likelihood component to the region-growing algorithm. The algorithm can be summarized in five steps. The image was first multiplied by a 2D shadow, whose size was approximately the same size as the ROI. We will henceforth refer to the image to which the 2D shadow has been applied as the "fuzzified" image. We started the threshold value at the maximum intensity in the image and decreased the intensities in successive steps. Consequently, we obtained a sequence of growing contours (S_i), where intensity value was the similarity criterion. There was an inverse relationship between intensity value and contour size, i.e., the lower the intensity value, the larger the contour. Next, we calculated the composite probability (P_i) for each contour (S_i):

$$P_i = p(S_i|pdf_i) \times p(outside S_i|ROI). \tag{1}$$

where $p(S_i|pdf_i)$ is the probability density function (pdf) of the ROI subject to the fuzzified image (see Fig. 1). This pdf is calculated *inside* the contour, S_i, where i is the thresholding step. The quantity $p(outside S_i|ROI)$ is the pdf of the ROI subject to the original image. This pdf is calculated *outside* the contour, S_i. Next we find the logarithm of the composite probability, P_i in the following way:

$$log(P_i) = log(p(S_i|pdf_i)) + log(p(outside S_i|ROI)), \tag{2}$$

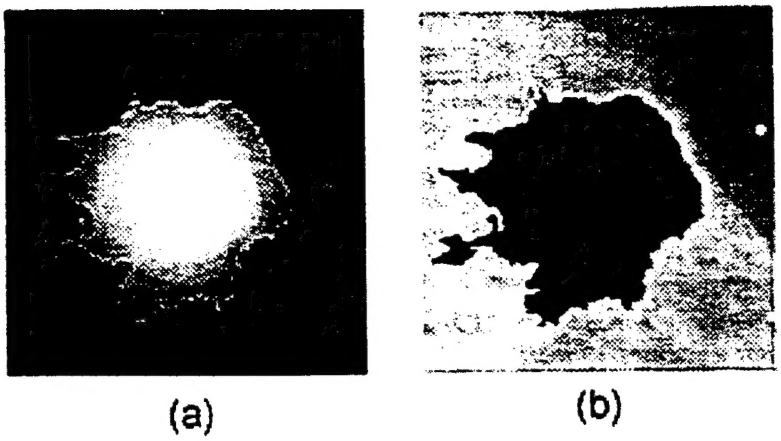

Figure 1: Figure (a) is used to calculate $p(S_i|pdf_i)$. Figure (b) is used to calculate $p(outsideS_i|ROI)$

Finally, we determine the likelihood that the contour represents the tumor body by assessing the maximum likelihood function:

$$argmax(Log(P_i)), \tag{3}$$

Equation 3 intends to find the maximum value of the aforementioned likelihood values as a function of intensity threshold. We assess (so as other investigators[5]) that the intensity value corresponding to this maximum likelihood value is the optimal intensity for the tumor body contour. We also determine the likelihood that the contour represents the tumor extended borders by assessing the maximum change of the likelihood function:

$$argmax(\frac{dLog(P_i)}{di}), \tag{4}$$

i.e., find the steepest jump on the aforementioned function. An intensity value between this jump and the maximum value on the function produces the best contour of the tumor body and its extended borders.

2.2. Feature Calculation

One extremely important task in the separation of malignant and benign tumors is feature selection and calculation. Benign tumors can be lucent at the center and can have well-defined borders; while malignant tumors can have spiculated and/or fuzzy borders. We used the following features:

Global Features

$$Skewness = \frac{1}{N}\frac{\sum_{i,j=0}^{N-1}[g(i,j) - \overline{g(i,j)}]^3}{\sqrt{\sum_{i,j=0}^{N-1}[g(i,j) - \overline{g(i,j)}]^3}} \tag{5}$$

where $g(i,j)$ is intensity value and $\overline{g(i,j)}$ is average intensity value.

$$Kurtosis = \frac{1}{N}\frac{\sum_{i,j=0}^{N-1}[g(i,j) - \overline{g(i,j)}]^4}{\sqrt{\sum_{i,j=0}^{N-1}[g(i,j) - \overline{g(i,j)}]^4}} \tag{6}$$

$$Circularity = \frac{A_1}{A}, \tag{7}$$

where A is the area of the actual ROI; A_1 is the area of the overlapped region of A and the effective circle A_c, which is defined as the circle whose area is equal to A and is centered at the corresponding centroid of A.

$$Compactness = \frac{p^2}{a}, \tag{8}$$

where, p=tumor perimeter and a=tumor area

$$perimeter = tumor\ perimeter. \tag{9}$$

Local Features

These intensity features were calculated on the 10° ROI as it was divided into 10° sectors in the polar coordinate system, therefore each tumor contained 36 sectors.

$$\overline{g(i,j)} = \frac{1}{N}\sum_{i,j=0}^{N-1} g(i,j), \tag{10}$$

where Mean $= \overline{g(i,j)}$, N is the total pixel number inside the ROI

$$Contrast = \frac{P_f - P_b}{P_f}, \tag{11}$$

where P_f is the average gray-level inside the ROI's and P_b is the average gray-level surrounding the ROI.

$$\sigma_f^2 = \frac{1}{N}\sum_{i=1}^{N}(g(i,j) - \overline{g(i,j)})^2, \tag{12}$$

where σ_f^2 = standard deviation.

$$Area = tumor\ area \tag{13}$$

$$\sigma_n = \frac{1}{N_b}\sum_{i=1}^{N_b}(r_i - \bar{r})^2, \tag{14}$$

where σ_n = Deviation of the Normalized Radial Length, N_b is the total number of pixels located on the boundary of the ROI, r_i is the value of the normalized radial length from the boundary coordinate (x_i, y_i) to the centroid of the ROI; $\bar{r}$ is the mean of r_i.

$$Roughness = ([\frac{1}{N_b}\sum_{i=1}^{N_b}(r_i - \bar{r})^4]^{\frac{1}{4}} - [\frac{1}{N_b}\sum_{i=1}^{N_b}(r_i - \bar{r})^2]^{\frac{1}{2}}])/\bar{r}. \tag{15}$$

$$radial\ length = length\ of\ radius, \tag{16}$$

where *length of radius* is the distance from the center of the tumor to its edge.

Given a second-order joint probability matrix $P_{d,\theta}(i,j)$, where $P_{d,\theta}(i,j)$ is the joint gray level distribution of a pixel pair (i,j) with the distance d and in the direction θ, six texture features are defined as follows:

$$E_{d,\theta}(i,j) = \sum_{i=1}^{L}\sum_{j=1}^{L} P_{d,\theta}(i,j)^2, \tag{17}$$

where $E_{d,\theta}(i,j)$ = energy.

$$I_{d,\theta}(i,j) = \sum_{i=1}^{L}\sum_{j=1}^{L}(i-j)^2 P_{d,\theta}(i,j), \tag{18}$$

where $I_{d,\theta}(i,j)$ = inertia.

$$E = \sum_{i=1}^{L}\sum_{j=1}^{L} P_{d,\theta}(i,j) log_2 P_{d,\theta}(i,j), \tag{19}$$

where E = entropy.

$$IDM_{d,\theta} = \sum_{i=1}^{L}\sum_{j=1}^{L}\frac{1}{1+(i-j)^2}P_{d,\theta}(i,j), \tag{20}$$

where, $IDM_{d,\theta}$ = Inverse Difference Moment.

$$DE_{d,\theta} = -\sum_{k=0}^{n-1} P_{x-y}(k) log_2 P_{x-y}(k), P_{x-y}(k) = \sum_{i=0}^{n-1}\sum_{j=0}^{n-1} P_{d,\theta}(i,j), \tag{21}$$

for $|i-j| = k, k = 0, 1, ..., n-1$ where, $DE_{d,\theta}$ = Difference Entropy.

2.3. Classifiers

We used a conventional backpropagation neural network for two of the three studies described in this paper. It is comprised of an input layer, one hidden layer, and one output. We used the multiple circular path neural network[8] for the third study described in this paper. It is comprised of 3 input layers, one hidden layer and one output. The first input layer is fully connected, i.e., all inputs connect to all hidden nodes. The second input layer is called a self correlation path, i.e., each node on the layer connects to a single set of the 18 image features for the fan-in and fully connects to the hidden nodes for fan-out. The third input layer is called a neighborhood correlation path, i.e., each node on the layer connects to the input nodes of adjacent sectors for the fan-in and fully connects to the hidden nodes for fan-out. Our study used 18 hidden layer nodes. A more detailed explanation of the MCPCNN can be found the work done by Lo et. al.[8].

3. EXPERIMENT

The image samples were chosen from several databases compiled by the ISIS Center of the Georgetown University (GU) Radiology Department and the University of Florida's Digital Database for Screening Mammography (DDSM).[3] They are a mixture of "obvious" cases and "not obvious" cases. The "obvious" cases contain tumors that are easily identifiable as malignant or benign while the "not obvious" cases are those that radiologists find difficult to observe and/or classify. Forty malignant and forty benign tumors were tested during this experiment. The GU films were digitized at a resolution of 100μm using a Lumiscan digitizer. The DDSM films were digitized at 43 and 50 μm's using both the Lumiscan and Howtek digitizers. We compensated for this difference in resolution by reducing the DDSM images to half their normal sizes. The images were of varying contrasts and the tumors were of varying sizes. There were 28 malignant cases and 23 benign cases.

The experiment was subdivided into three studies as shown in table 1 below.

Experiments 1 and 2 used 6 global and 12x36 sector features to yield a total of 438 image features per tumor. There were 18 hidden nodes and 1 output for both the BP and MCPCNN classifiers. The training and testing method used was the jackknife method. Experiment 3 used 19 likelihood feature values per tumor. There were 15 hidden nodes and 1 output for the BP classifier. The training and testing method used was the jackknife method. The results were analyzed using the LABROC4 program.[10]

Experiment	Features	Neural Network
1	Image Features	Conventional NN
2	Image Features	MCPCNN
3	ML-curve as features	Conventional NN

Table 1: This table summarizes the studies presented in this paper.

4. RESULTS

Here are two examples of segmentation results for both malignant (see Fig. 2) and benign (see Fig. 4) cases. Each example gives the segmentation result produced by the maximum likelihood value on the curves described in section 2.1.

The following is a table, which gives the A_z values produced by the neural network.

Experiment	Features	Neural Network	Az
1	Image Features	Conventional NN	0.66
2	Image Features	MCPCNN	0.71
3	ML-curve as features	Conventional NN	0.84

Table 2: Results from Experiments 1-3.

5. CONCLUSION AND DISCUSSION

In analyzing the segmentation results we drew several conclusions. We discovered that there was a marked difference between the likelihood functions in malignant cases and the likelihood functions in benign cases. The likelihood function in the benign case often experiences a sharp drop, while the likelihood function in the malignant case is often smoother. In the image, a sharp drop value in the likelihood function represents an abrupt change in the area as well as likelihood value. We observed thatin benign cases, the likelihood function sharp changes are much more evident because benign tumors usually have well-defined borders. Conversely, in many malignant cases, the likelihood functions are smoother because many of their the borders are ill-defined. In analyzing the likelihood functions for malignant cases we recognized that those curves with very sharp changes were produced from tumors with well-defined borders and vice versa; i.e., there were malignant tumors that could be mistaken as benign and vice versa.

The maximum likelihood curves used as inputs to the BP neural network produced the best performance overall. The image features used as inputs to the MCPCNN produced the second best performance. The image features used as inputs to the BP produced the worst performance. Since we received the best results by using the likelihood functions as features, we expect that the MCPCNN may improve the overall results by giving the likelihood functions in every sector.

ACKNOWLEDGMENTS

This work has been supported by the following grants: DAMD17-00-1-0291, DAAG55-98-1-0187, and DAMD17-00-1-0267.

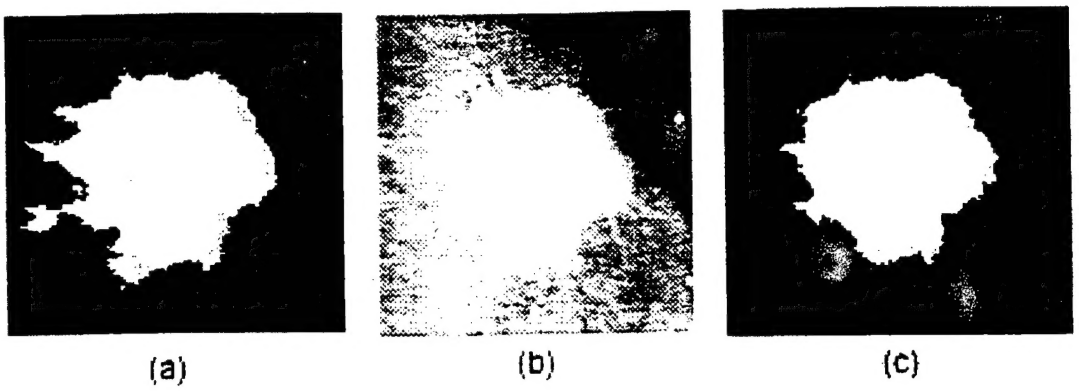

Figure 2. The segmentation results for a malignant tumor. Part (a) shows the segmentation result produced by the maximum likelihood change intensity choice, part (b) shows the original image, and part (c) shows the segmentation result produced by the maximum likelihood intensity choice.

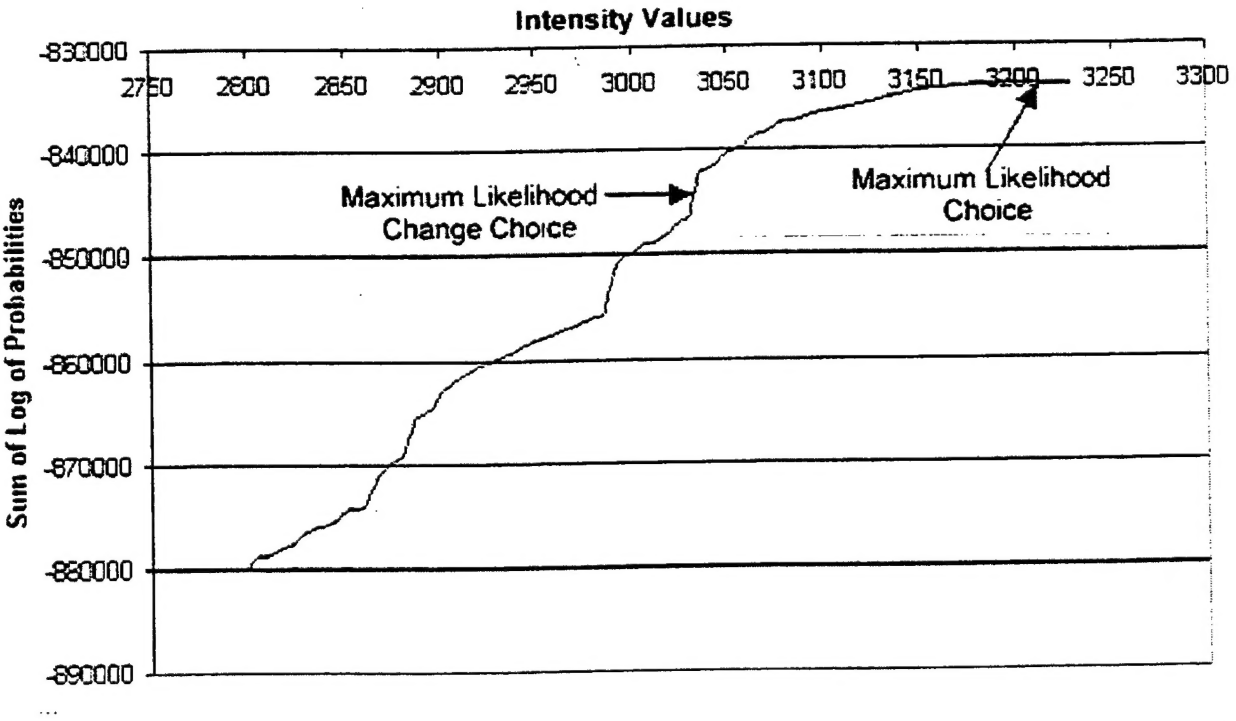

Figure 3. A likelihood function with respect to threshold values for all segmentation steps (malignant case) shown in Fig. 2.

REFERENCES

1. Frankel SD, Sickel EA, Curpen BN, Sollito RA, Ominsky SH. Galvin HB, *Initial versus subsequent screening mammography: Comparison of findings and their prognostics significance.* AJR, 1995, vol. 164, pp. 1107-1109.
2. Gonzalez RC, Woods RE. Digital Image Processing Reading, MA: Addison Wesley, 1992.

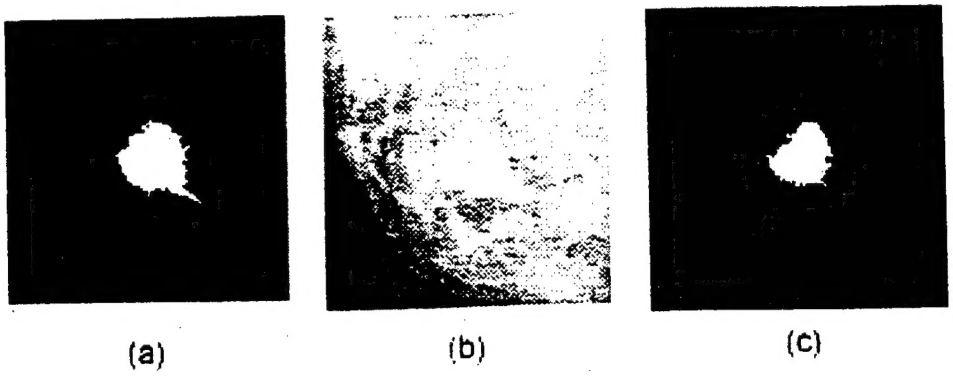

Figure 4. The segmentation results for a benign tumor. Part (a) shows the segmentation result produced by the maximum likelihood change intensity choice, part (b) shows the original image, and part (c) shows the segmentation result produced by the maximum likelihood intensity choice.

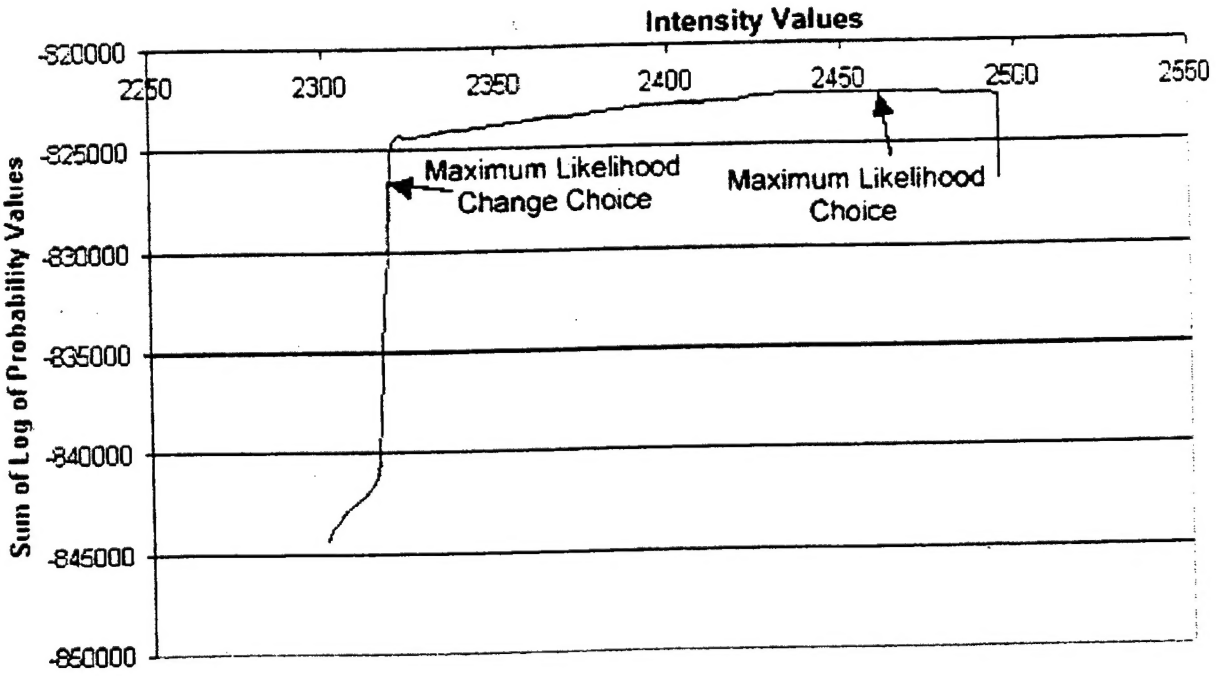

Figure 5. A likelihood function with respect to threshold values for all segmentation steps (benign case) shown in Fig. 4.

3. Heath M, Bowyer KW, Kopans D et al, *Current status of the Digital Database for Screening Mammography*, Digital Mammography, Kluwer Academic Publishers, 1998, pp. 457-460.
4. Kopans DB. *The positive predictive value of mammography*, AJR, 1991, vol. 158, pp. 521-526.
5. Kupinski MA, Giger ML, *Automated Seeded Lesion Segmentation on Digital Mammograms*, IEEE Transactions on Medical Imaging, 1998, vol. 17, no. 4, pp. 510-517.
6. Li L, Zheng Y, Zhang L, Clark R, *False-positive reduction in CAD mass detection using a competitive classification strategy*, Medical Physics, 2001, Vol. 28, no. 2, pp. 250-258.

7. Li H, Wang Y, Liu KJR, Lo S-C, Freedman MT, *Computerized Radiographic Mass Detection - Part I: Lesion Site Selection by Morphological Enhancement and Contextual Segmentation*, IEEE Transactions on Medical Imaging, 2001, vol. 20, no. 4, pp. 289-301.
8. Lo SC, Li H, Wang J, Kinnard L, Freedman MT, *A Multiple Circular Path Convolution Neural Network System for Detection of Mammographic Masses*, IEEE Transactions on Medical Imaging, 2002, vol. 21, No. 2, (Accepted for publication).
9. Mendez AJ, Tahoces PG, Lado MJ, Souto M., Vidal JJ, *Computer-aided diagnosis: Automatic detection of malignant masses in digitzed mammograms*, Medical Physics, 1998, vol. 25, no. 6, pp. 957-964.
10. Metz C, LABROC Program, ftp://radiology.uchicago.edu/roc.
11. Nystrom L, Rutqvist LE, Wall S, Lindgren A, Lindqvist M, Ryden S, et. al., *Breast cancer screening with mammography: Overview of Swedish randomized trials*, Lancet, 1993, vol. 341, pp. 973-978.
12. Petrick N, Chan H-P, Sahiner B, Wei D, *An Adaptive Density-Weighted Contrast Enhancement Filter for Mammographic Breast Mass Detection*, IEEE Transactions on Medical Imaging, 1996, vol. 15, no. 1, pp. 59-67.
13. Pohlman S, Powell KA, Obuchowski NA, Chilcote WA, Grundfest-Broniatowski S, *Quantitative classification of breast tumors in digitized mammograms*, Medical Physics, 1996, vol. 23, no. 8, pp. 1336-1345.
14. Sahiner B, Chan HP, Wei D, Petrick N, Helvie MA, Adler DD, Goodsit MM, *Image feature selection by a genetic algorithm: Application to classification of mass and normal breast tissue*, Medical Physics, 1996, vol. 23, no. 10, pp. 1671-1684.
15. Shapiro S, *Screening: Assessment of current studies*, Cancer, 1994, vol. 74, pp.231-238.
16. Tabar L, Fagerberg G, Duffy S, Day NE, Gad A, Grontoft O. *Update of the Swedish two-country program of mammographic screening for breast cancer*, Radiology Clinics of North America: Breast Imaging - Current Status and Future Directions, 1992, vol. 30, pp. 187-210.

SEMINARS

Time: 12:40 pm
Place: Electrical Engineering Department

1/15	A Mammography SoftCopy Display Workstation for Breast Cancer Research	By Dr. Jerry Gaskil
1/29	Mammography 101 - A (Mammography Physics and Image Requirements)	By Dr. S-C. Ben Lo
2/12	Mammography 101 - B (Mammography Physics and Image Requirements)	By Dr. S-C. Ben Lo
2/22	Ultrasound Instrumentation (State-of-the-art Breast Ultrasound) This seminar will be held 8:30 am -> 9:30 am Feburary 22nd at the ISIS Center GUMC. (Suite 603, 2115 Wisconsin Ave., N.W., DC)	By Mr. Terry Correll
2/26	Cancer biology and physiology	By Dr. Theodore Bremner
3/12	Breast Cancer Oncology and Management	By Dr. Theodore Bremner
3/26	Human Breast Anatomy	By Dr. Matthew Freedman
4/09	Breast Ultrasound	By Ms. Anita Sarcone
4/23	MRI in Breast Cancer	By Dr. Paul Wang